Article

PNA versus DNA: Effects of Structural Fluctuations on Electronic Structure and Hole-Transport Mechanisms

Elizabeth Hatcher, Alexander Balaeff, Shahar Keinan, Ravindra Venkatramani, and David N. Beratan

J. Am. Chem. Soc., **2008**, 130 (35), 11752-11761 • DOI: 10.1021/ja802541e • Publication Date (Web): 12 August 2008

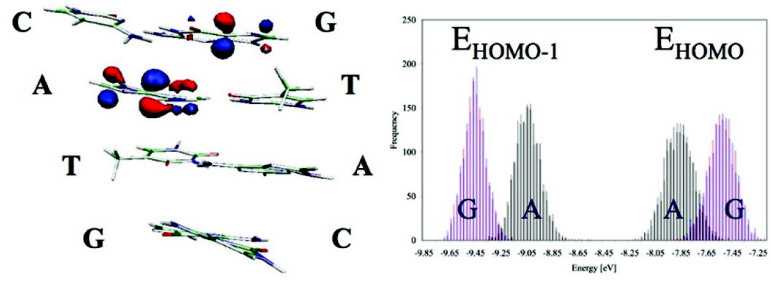

More About This Article

Additional resources and features associated with this article are available within the HTML version:

- Supporting Information
- Links to the 1 articles that cite this article, as of the time of this article download
- Access to high resolution figures
- Links to articles and content related to this article
- Copyright permission to reproduce figures and/or text from this article

View the Full Text HTML

J|A|C|S
ARTICLES

Published on Web 08/12/2008

PNA versus DNA: Effects of Structural Fluctuations on Electronic Structure and Hole-Transport Mechanisms

Elizabeth Hatcher, Alexander Balaeff, Shahar Keinan, Ravindra Venkatramani, and David N. Beratan*

Department of Chemistry, Duke University, French Family Science Center, Durham, North Carolina 27708

Received April 10, 2008; E-mail: david.beratan@duke.edu

Abstract: The effects of structural fluctuations on charge transfer in double-stranded DNA and peptide nucleic acid (PNA) are investigated. A palindromic sequence with two guanine bases that play the roles of hole donor and acceptor, separated by a bridge of two adenine bases, was analyzed using combined molecular dynamics (MD) and quantum-chemical methods. Surprisingly, electronic structure calculations on individual MD snapshots show significant frontier orbital electronic population on the bridge in ~10% of the structures. Electron-density delocalization to the bridge is found to be gated by fluctuations of the covalent conjugated bond structure of the aromatic rings of the nucleic bases. It is concluded, therefore, that both thermal hopping and superexchange should contribute significantly to charge transfer even in short DNA/PNA fragments. PNA is found to be more flexible than DNA, and this flexibility is predicted to produce larger rates of charge transfer.

Introduction

Charge transfer (CT) in DNA is a topic of great recent interest and debate.[1−9] CT has been suggested to influence protein−DNA interactions in vivo and to play a role in DNA repair.[10,11] Future nanotechnology applications may use DNA as an electronic conduit.[2,12] Many DNA CT experiments employ positive charge carriers (holes). A hole in DNA attains its lowest energy when it is localized on a guanine base (G) or delocalized over several consecutive G's. The energy of a hole localized on any other base is higher, by ~0.2 eV ($8k_BT$) for adenine (A) and ~0.6 eV ($24k_BT$) for either thymine (T) or cytosine (C), where k_B is Boltzmann's constant and the temperature T is 300 K (see ref 2 and references therein). Therefore, from the CT perspective, Gs of GC base pairs (BPs) are believed to play the role of hole traps (donors and acceptors), and stretches of AT BPs between the Gs are believed to play the role of barriers (bridges) between the traps, which are visited by the holes only transiently. It is useful to distinguish between DNA CT in bridges with large versus small barrier heights.[6,13] Indeed, a diversity of mechanisms associated with these differences was observed in early experiments.[14−18] Moreover, transitions among mechanisms can likely be induced, as indicated by a tunneling-energy dependence of the distance dependence of the ET rate as bridge states approach resonance with those of the donor and acceptor.[19,20]

Experimental studies have shown that the rate of hole transfer between donor−acceptor pairs (G's or stilbene moieties covalently attached to DNA[21,22]) decays with increasing bridge length. For bridges with lengths of 1−3 BP, the measured CT rates decrease approximately exponentially with distance. However, when the distance exceeds 3 BP, the rate decreases very slowly with distance.[4,23] It has been suggested that this change indicates a switching in the dominant mechanism of hole transfer. For short donor−acceptor separation distances, the charge is believed to be transferred via direct superexchange

(1) Augustyn, K. E.; Genereux, J. C.; Barton, J. K. *Angew. Chem., Int. Ed.* **2007**, *46*, 5731–5733.
(2) Endres, R. G.; Cox, D. L.; Singh, R. R. P. *Rev. Mod. Phys.* **2004**, *76*, 195–214.
(3) Giese, B.; Biland, A. *Chem. Commun.* **2002**, 667–672.
(4) Lewis, F. D.; Zhu, H. H.; Daublain, P.; Fiebig, T.; Raytchev, M.; Wang, Q.; Shafirovich, V. *J. Am. Chem. Soc.* **2006**, *128*, 791–800.
(5) Barnett, R. N.; Cleveland, C. L.; Joy, A.; Landman, U.; Schuster, G. B. *Science* **2001**, *294*, 567–571.
(6) Berlin, Y. A.; Kurnikov, I. V.; Beratan, D.; Ratner, M. A.; Burin, A. L. In *Long-Range Charge Transfer in DNA II*; Schuster, G. B., Ed.; Topics in Current Chemistry, Vol. 237; Springer: Berlin/Heidelberg, 2004; pp 1−36.
(7) Nitzan, A.; Ratner, M. A. *Science* **2003**, *300*, 1384–1389.
(8) Beratan, D. N.; Priyadarshy, S.; Risser, S. M. *Chem. Biol.* **1997**, *4*, 3–8.
(9) Netzel, T. L. *J. Biol. Inorg. Chem.* **1998**, *3*, 210–214.
(10) Kanvah, S.; Schuster, G. B. *Pure Appl. Chem.* **2006**, *78*, 2297–2304.
(11) Hall, D. B.; Holmlin, R. E.; Barton, J. K. *Nature* **1996**, *382*, 731–735.
(12) Dekker, C.; Ratner, M. A. *Phys. World* **2001**, *14*, 29–33.
(13) Priyadarshy, S.; Risser, S. M.; Beratan, D. N. *J. Phys. Chem.* **1996**, *100*, 17678–17682.
(14) Wan, C. Z.; Fiebig, T.; Schiemann, O.; Barton, J. K.; Zewail, A. H. *Proc. Natl. Acad. Sci. U.S.A.* **2000**, *97*, 14052–14055.
(15) Meade, T. J.; Kayyem, J. F. *Angew. Chem., Int. Ed. Engl.* **1995**, *34*, 352–354.
(16) Lewis, F. D.; Wu, T. F.; Zhang, Y. F.; Letsinger, R. L.; Greenfield, S. R.; Wasielewski, M. R. *Science* **1997**, *277*, 673–676.
(17) Schuster, G. B. *Acc. Chem. Res.* **2000**, *33*, 253–260.
(18) Giese, B. *Annu. Rev. Biochem.* **2002**, *71*, 51–70.
(19) Lewis, F. D.; Liu, J. Q.; Weigel, W.; Rettig, W.; Kurnikov, I. V.; Beratan, D. N. *Proc. Natl. Acad. Sci. U.S.A.* **2002**, *99*, 12536–12541.
(20) Skourtis, S. S.; Beratan, D. N.; Onuchic, J. N. *Chem. Phys.* **1993**, *176*, 501–520.
(21) Buchvarov, I.; Wang, Q.; Raytchev, M.; Trifonov, A.; Fiebig, T. *Proc. Natl. Acad. Sci. U.S.A.* **2007**, *104*, 4794–4797.
(22) Giese, B. *Curr. Opin. Chem. Biol.* **2002**, *6*, 612–618.
(23) Giese, B.; Amaudrut, J.; Kohler, A. K.; Spormann, M.; Wessely, S. *Nature* **2001**, *412*, 318–320.

10.1021/ja802541e CCC: $40.75

Scheme 1. DNA and PNA Structures: (A) Chemical Structures of the DNA and PNA Backbones; (B) Arrangement of Nucleic Base Pairs in the Helical Stacks in B-DNA, A-DNA, and PNA[a]

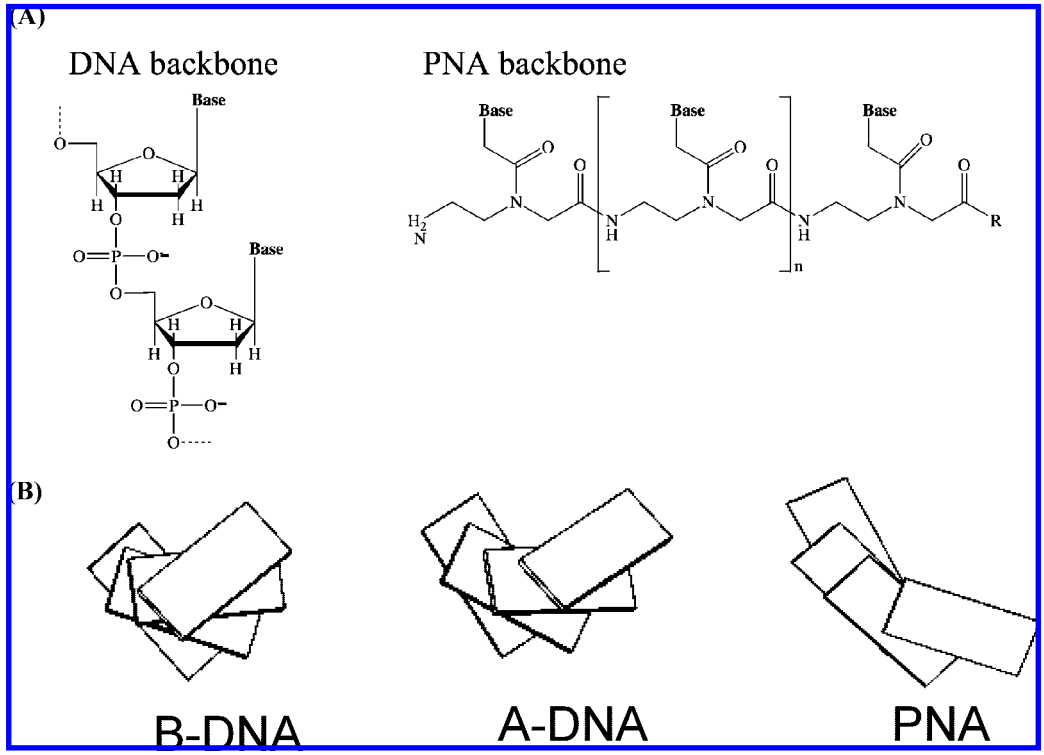

[a] This scheme was made using X3DNA.[71] The DNA structures were built using the online tool *model.it*.[47] The PNA structure, built as described in Methods, was taken from our MD simulation.

(tunneling) from donor to acceptor without populating the intermediate A bases of the bridge. For longer separations, the rate of superexchange becomes negligible, and the hopping mechanism, whereby the hole is transferred from donor to acceptor through bridge-localized intermediate states, dominates.

The dynamical nature of DNA and its environment (water, counterions) further complicates the CT mechanism. For long DNA sequences, polaron-assisted hopping mechanisms have been suggested to play a role in CT.[24−27] Furthermore, thermal fluctuations shift the hole energies and change the coupling between neighboring bases. The dependence of DNA CT rates on temperature suggests that the CT is conformationally gated.[28] Indeed, simulations have indicated that ionic motion may gate hole transfer in DNA.[5] Recently, it was shown that thermal fluctuations of DNA can significantly change V_{DA}, the coupling between the hole donor and acceptor,[29,30] a well-studied phenomenon in proteins.[31,32] A detailed understanding of how DNA dynamics couples to CT remains incomplete.

Developing a theoretical analysis for the effects of DNA dynamics on CT presents a formidable challenge. Accurately modeling the quantum dynamics of DNA in the condensed phase is prohibitively costly; one must rely on a range of approximations and simplifying assumptions. One way to estimate V_{DA} is to use the multistate generalized Mulliken−Hush (GMH) method.[29,33−35] The method describes donor−acceptor interaction mediated by the bridge. In the case of DNA, the GMH method was shown to be preferable to the classic two-state Mulliken−Hush strategy because of the closeness of the donor/acceptor and bridge energy levels.[29]

Another candidate for CT studies that is closely related to DNA is peptide nucleic acid (PNA).[36−39] PNA contains the same Watson−Crick BPs as DNA, but the bases are connected by a pseudopeptide rather than a sugar−phosphate backbone (Scheme 1). The PNA bases form a helical π stack similar to the one in DNA, suggesting that PNA may also support hole conduction. Indeed, recent experiments have found CT in PNA that is reminiscent of CT in DNA.[40,41] However, the significant geometric and physical differences between PNA and DNA may

(24) Kurnikov, I. V.; Tong, G. S. M.; Madrid, M.; Beratan, D. N. *J. Phys. Chem. B* **2002**, *106*, 7–10.
(25) Schuster, G. B.; Landman, U. In *Long-Range Charge Transfer in DNA I*; Schuster, G. B., Ed.; Topics in Current Chemistry, Vol. 236; Springer: Berlin/Heidelberg, 2004; pp 139−161.
(26) Rakhmanova, S. V.; Conwell, E. M. *J. Phys. Chem. B* **2001**, *105*, 2056–2061.
(27) (a) *Long-Range Charge Transfer in DNA I*; Schuster, G. B., Ed.; Topics in Current Chemistry, Vol. 236; Springer: Berlin/Heidelberg, 2004. (b) *Long-Range Charge Transfer in DNA II*; Schuster, G. B., Ed.; Topics in Current Chemistry, Vol. 237; Springer: Berlin/Heidelberg, 2004.
(28) O'Neill, M. A.; Becker, H. C.; Wan, C.; Barton, J. K.; Zewail, A. H. *Angew. Chem., Int. Ed.* **2003**, *42*, 5896–5900.
(29) Voityuk, A. A. *Chem. Phys. Lett.* **2007**, *439*, 162–165.
(30) Troisi, A.; Orlandi, G. *J. Phys. Chem. B* **2002**, *106*, 2093–2101.
(31) Skourtis, S. S.; Balabin, I. A.; Kawatsu, T.; Beratan, D. N. *Proc. Natl. Acad. Sci. U.S.A.* **2005**, *102*, 3552–3557.
(32) Wolfgang, J.; Risser, S. M.; Priyadarshy, S.; Beratan, D. N. *J. Phys. Chem. B* **1997**, *101*, 2986–2991.
(33) Cave, R. J.; Newton, M. D. *Chem. Phys. Lett.* **1996**, *249*, 15–19.
(34) Voityuk, A. A. *J. Phys. Chem. B* **2005**, *109*, 17917–17921.
(35) Voityuk, A. A.; Rosch, N.; Bixon, M.; Jortner, J. *J. Phys. Chem. B* **2000**, *104*, 9740–9745.
(36) Rasmussen, H.; Kastrup, J. S.; Nielsen, J. N.; Nielsen, J. M.; Nielsen, P. E. *Nat. Struct. Biol.* **1997**, *4*, 98–101.
(37) Egholm, M.; Buchardt, O.; Christensen, L.; Behrens, C.; Freier, S. M.; Driver, D. A.; Berg, R. H.; Kim, S. K.; Norden, B.; Nielsen, P. E. *Nature* **1993**, *365*, 566–568.
(38) Egholm, M.; Nielsen, P. E.; Buchardt, O.; Berg, R. H. *J. Am. Chem. Soc.* **1992**, *114*, 9677–9678.
(39) Nielsen, P. E.; Egholm, M.; Berg, R. H.; Buchardt, O. *Science* **1991**, *254*, 1497–1500.

produce different CT characteristics. The structural differences include the smaller twist of the PNA double helix, the larger π overlap between the neighboring bases in PNA (see Scheme 1), and the electrostatic charge of the DNA backbone that attracts a significant number of counterions.

Here we present an in-depth analysis of how the structural dynamics of both DNA and PNA affect the electronic structure of the π stack. We used molecular dynamics (MD) simulations to generate ensembles of double-stranded DNA and PNA conformations for the palindromic sequence CATG. The electronic structures of these conformations were computed, and the nonadiabatic couplings between the hole donor and acceptor states were calculated using the GMH strategy. In agreement with the earlier studies,[29,30] we found that thermal fluctuations can significantly increase the donor−acceptor superexchange interaction in both DNA and PNA. However, we also found that in ∼10% of the MD structures, the highest occupied molecular orbitals (HOMOs) are delocalized between the donor/acceptor Gs and the bridging As, indicating that the hole in those structures is likely to be similarly delocalized. This delocalization suggests a significant contribution of hopping transport to the CT kinetics, even over short distances (2 BP in the present case). Comparison of PNA and DNA structures shows PNA to be more flexible than DNA and therefore more likely to adopt conformations favoring CT by either hopping or superexchange.

Methods

Conformational ensembles of DNA and PNA molecules with the palindromic sequence 5′-GGCATGCC-3′ were generated using MD simulations. Next, the electronic structure of each CATG core segment was analyzed using a semiempirical INDO/s method.[42] The orbital energies and electron densities for HOMO through HOMO-6 as well as the electronic coupling V_{DA} between the hole states on the two G's of the core segment were computed. The rate of superexchange hole transfer between the G's is proportional to $\langle V_{DA}^2 \rangle$.[43,44]

The MD simulations were performed using the AMBER8 program and the AMBER99 forcefield, the NPT ensemble (1 atm, 300 K), particle-mesh Ewald (P3ME) electrostatics, and periodic boundary conditions. The DNA and PNA segments were solvated in a bath of TIP3P waters; Na^+ counterions were added to the DNA system to retain charge neutrality. The total system size was 27 350 atoms for DNA and 35 292 atoms for PNA. The lengths of all chemical bonds between hydrogens and heavy atoms were constrained in the simulation using the SHAKE/RATTLE method.[45,46] The initial structure of the canonical B-DNA was constructed using the online tool *model.it*.[47] The initial structure of PNA was constructed by modifying the PNA hexamer crystal structure of Rasmussen and Kastrup[36] (PDB code 1PUP). The nucleotide bases of the 1PUP sequence CGTACG were mutated toward the desired sequence GCATGC using VMD,[48] and one GC base pair was added to each end of the sequence. The atomic charges for PNA were computed using the RESP method,[49] and these charges were found to be close to those used in other simulations[50] (see the Supporting Information).

The simulations were run for 1.5 ns, and 1500 coordinate frames were saved for each system (1 frame/ps). This sampling strategy is different from that adopted in previous studies. For example, Voityuk[29] sampled ∼10 000 structures in a 10 ps trajectory. Our sampling protocol was chosen for two reasons. First, the sampling time of 1 ps significantly exceeds the fluctuation time of the electronic couplings in DNA, which are estimated to be in the range 10−20 fs.[29,30,51] Therefore, the sampled electronic structures were uncorrelated. Second, sampling over 1.5 ns allowed us to probe somewhat larger-scale motions of DNA and PNA that are not accessible on the picosecond time scale and to evaluate the influence of these motions on the electronic structure.

For each MD snapshot, the atomic coordinates of the eight bases of the core segment CATG were extracted, and the dangling bonds were capped with hydrogens using VMD. In what follows, the eight bases will be labeled as $C_1A_1T_1G_1{:}C_2A_2T_2G_2$. The electronic structure of the core segment was calculated with the INDO/s method implemented in the CNDO program.[52] The semiempirical INDO/s approach provides a useful balance between cost and performance,[42] especially for electronic structures with a strong propensity for CT, where density functional theory methods may fail.[53] The application of quantum-chemical methods to compute the donor−acceptor coupling in DNA has been reviewed previously,[54] and it was found that the INDO/s results agree well with higher-level calculations (such as CASPT2 and CASSCF[55]). INDO/s calculations are at least 2 orders of magnitude faster than the higher-level calculations, making them indispensable for dealing with thousands of MD snapshots.

On the basis of Koopmans' theorem, the HOMO and HOMO-1 obtained from the INDO/s calculations correspond to the CT-active species, i.e., the hole donor and acceptor states.[29,54] The orbitals HOMO-2, HOMO-3, etc., include bridge orbitals that mediate superexchange. Through the use of single-point self-consistent field calculations with the INDO/s Hamiltonian, the electronic coupling V_{DA} between the donor and acceptor states (equal to the coupling V_{12} between the HOMO and HOMO-1) was computed by the GMH method:[56,57]

$$V_{DA} = V_{12} = (E_2 - E_1)\frac{\mu_{12}}{\sqrt{(\mu_1 - \mu_2)^2 + 4\mu_{12}^2}} + \sum_{j=3}^{n}\left(E_j - \frac{E_1 + E_2}{2}\right)\frac{\mu_{1j}\mu_{2j}}{\sqrt{[(\mu_j - \mu_1)^2 + 4\mu_{1j}^2][(\mu_2 - \mu_j)^2 + 4\mu_{2j}^2]}} \quad (1)$$

where E_j and μ_j are the electronic energy and dipole moment for orbital j and μ_{ij} is the transition dipole moment between orbitals i and j. The diabatic electronic states are replaced with orbitals (1 = HOMO, 2 = HOMO-1, 3 = HOMO-2, etc.), and n is the total number of orbitals included in the multistate method. Replacing states with orbitals[29,58] allows the coupling element for hole transfer to be calculated from ground-state (neutral) structures, eliminating

(40) Wei, H.; Hatcher, E.; Balaeff, A.; Beratan, D. N.; Gil, R. R.; Madrid, M.; Achim, C. *J. Am. Chem. Soc.*, 2008, in press.
(41) Paul, A.; Watson, R. M.; Lund, P.; Xing, Y.; Burke, K.; He, Y.; Borguet, E.; Achim, C.; Waldeck, D. H. *J. Phys. Chem. C* **2008**, *112*, 7233–7240.
(42) Ridley, J.; Zerner, M. *Theor. Chim. Acta* **1973**, *32*, 111–134.
(43) Jortner, J.; Bixon, M.; Voityuk, A. A.; Rosch, N. *J. Phys. Chem. A* **2002**, *106*, 7599–7606.
(44) Troisi, A.; Nitzan, A.; Ratner, M. A. *J. Chem. Phys.* **2003**, *119*, 5782–5788.
(45) Ryckaert, J.-P.; Ciccotti, G.; Berendsen, H. J. C. *J. Comput. Chem.* **1977**, *23*, 327–341.
(46) Andersen, H. C. *J. Comput. Phys.* **1983**, *52*, 24–34.
(47) Munteanu, M. G.; Vlahovicek, K.; Parthasarathy, S.; Simon, I.; Pongor, S. *Trends Biomol. Sci.* **1998**, *23*, 341–347.
(48) Humphrey, W.; Dalke, A.; Schulten, K. *J. Mol. Graphics* **1996**, *14*, 33–38.
(49) Bayly, C. I.; Cieplak, P.; Cornell, W. D.; Kollman, P. A. *J. Phys. Chem.* **1993**, *97*, 10269–10280.
(50) Shields, G. C.; Laughton, C. A.; Orozco, M. *J. Am. Chem. Soc.* **1999**, *121*, 1625.
(51) Grozema, F. C.; Tonzani, S.; Berlin, Y. A.; Schatz, G. C.; Siebbeles, L. D. A.; Ratner, M. A. *J. Am. Chem. Soc.* **2008**, *130*, 5157–5166.
(52) Zeng, J.; Hush, N. S.; Reimers, J. R. *J. Am. Chem. Soc.* **1996**, *118*, 2059–2068.
(53) Hutchison, G. R.; Ratner, M. A.; Marks, T. J. *J. Phys. Chem. A* **2002**, *106*, 10596–10605.
(54) Rosch, N.; Voityuk, A. A. *Top. Curr. Chem.* **2004**, *237*, 37–72.
(55) Voityuk, A. A. *Chem. Phys. Lett.* **2006**, *427*, 177–180.
(56) Voityuk, A. A. *Chem. Phys. Lett.* **2006**, *422*, 15–19.
(57) Cave, R. J.; Newton, M. D. *J. Chem. Phys.* **1997**, *106*, 9213–9226.
(58) Voityuk, A. A. *J. Chem. Phys.* **2005**, *123*, 034903.

the need to compute the excited states (doublet cations). Excited-state approaches may in fact result in large errors because the GMH method is likely to exaggerate the electron-density decrease at the cation site, especially in the absence of the mitigating effects of the environment. The rule of thumb for the aromatic stacks of DNA and PNA is to use the GMH method with $2K + 2$ states, where K is the number of bridging BPs.[56] Therefore, six bridge states were used in eq 1 for the CATG segment.

Results and Discussion

We first summarize the results of our MD simulations and electronic-coupling computations. Next, we demonstrate that a few surprisingly large V_{DA} values result from the delocalization of the hole donor and acceptor states, and we explore the structural origins of that delocalization. Finally, we compare the results obtained for PNA and DNA and discuss their implications for hole transport in these two molecules.

A. PNA Has Greater Structural Flexibility than DNA. The ensembles of 1500 structures of the DNA and PNA octamers collected during the 1.5 ns MD simulations provide a good sampling of both the fluctuations of the chemical structures of individual nucleic bases (10 fs−10 ps time scale[29,30,51]) and the changes in relative positions and orientations of neighboring BPs (1−10 ps time scale[59−61]). The latter fluctuations are usually characterized using helicoidal parameters: roll, tilt, twist, shift, slide, and rise.[62] Sampling slower collective motions, such as the undulations of the whole octamer, as well as rare events such as flipping of the bases in and out of the nucleic acid stack would require sampling times that are orders of magnitude longer.[59−61] The influence of such longer-time-scale motions on the CT properties of DNA and PNA is beyond the scope of this investigation.

The maps of root-mean square deviations (RMSDs) of the structures of the CATG core segment were computed for the collected DNA and PNA ensembles (see the Supporting Information). The maps reveal large basins of similar structures, showing that the fluctuations of the octamers were indeed mostly local and that deviations from the average structures were rare. The DNA structures from the basins of stability correspond to B-form DNA (B-DNA), whereas the PNA structures are more reminiscent of A-form DNA (A-DNA), as expected (see Scheme 1 and Table 1).

Overall, the PNA segment shows more structural flexibility than does the DNA segment, as characterized by larger average RMSDs (more frequent fluctuations away from the basins). The helicoidal parameters of DNA have smaller standard deviations than those of PNA and are mostly distributed around single peaks, whereas the PNA parameters show wider distributions (see Table 1). At 820 ps in the PNA trajectory, a rare event occurred: a sudden slide of the C_1:G_2 base pair with respect to the A_1:T_2 base pair by more than 2 Å. The distorted state persisted for ~220 ps. That particular conformational change, however, had little influence on the mean squared electronic coupling (see section D of the Results and the Supporting Information). The increased structural flexibility of PNA is attributed to a more flexible backbone, in accord with earlier observations.[40,63,64]

Table 1. Average Values and Standard Deviations for the Helicoidal Parameters for Each Base Step in the Modeled CATG DNA/PNA Sequence[a]

		DNA	PNA
roll (deg)	C_1:G_2//A_1:T_2	11.38 ± 6.26	3.62 ± 7.13
	A_1:T_2//T_1:A_2	1.77 ± 5.18	2.05 ± 4.87
	T_1:A_2//G_1:C_2	11.17 ± 6.15	2.56 ± 6.52
tilt (deg)	C_1:G_2//A_1:T_2	0.93 ± 4.87	1.14 ± 5.65
	A_1:T_2//T_1:A_2	−0.28 ± 3.94	0.46 ± 4.89
	T_1:A_2//G_1:C_2	−0.82 ± 4.94	−1.18 ± 5.35
twist (deg)	C_1:G_2//A_1:T_2	32.75 ± 5.79	18.76 ± 7.05
	A_1:T_2//T_1:A_2	28.54 ± 4.75	6.60 ± 7.59
	T_1:A_2//G_1:C_2	30.68 ± 5.35	20.94 ± 7.03
shift (Å)	C_1:G_2//A_1:T_2	−0.06 ± 0.63	−0.69 ± 0.64
	A_1:T_2//T_1:A_2	−0.01 ± 0.65	−0.13 ± 0.58
	T_1:A_2//G_1:C_2	0.06 ± 0.61	0.97 ± 0.64
slide (Å)	C_1:G_2//A_1:T_2	−0.62 ± 0.57	−3.23 ± 0.86
	A_1:T_2//T_1:A_2	−0.87 ± 0.43	−2.86 ± 0.37
	T_1:A_2//G_1:C_2	−0.51 ± 0.66	−2.89 ± 0.68
rise (Å)	C_1:G_2//A_1:T_2	3.46 ± 0.37	3.46 ± 0.49
	A_1:T_2//T_1:A_2	3.20 ± 0.26	3.07 ± 0.31
	T_1:A_2//G_1:C_2	3.34 ± 0.39	3.37 ± 0.47

[a] The parameters were calculated with X3DNA[71] for DNA and PNA for each 1 ps snapshot along a 1.5 ns trajectory.

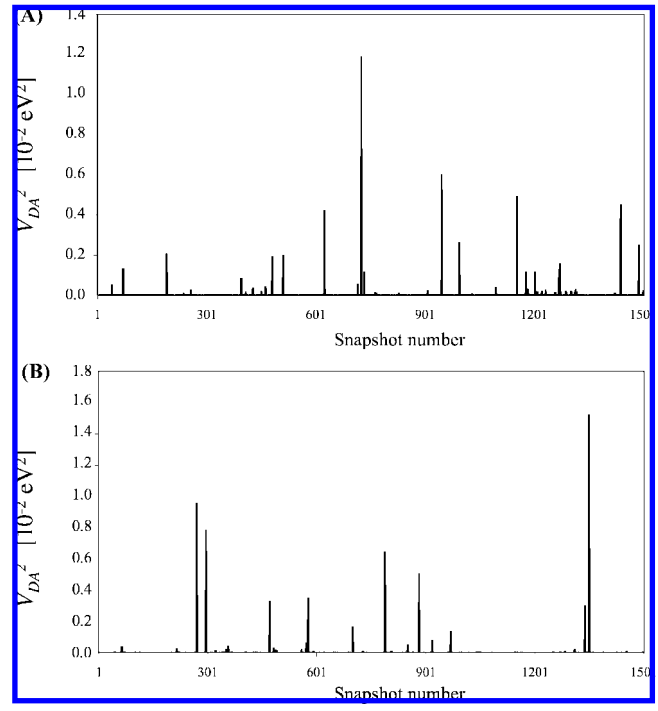

Figure 1. Electronic couplings V_{DA}^2 calculated from the six-state GMH formula (eq 1) for snapshots taken every 1 ps along a 1.5 ns MD trajectory: (A) DNA, (B) PNA.

B. Sensitivity of Electronic Coupling to Thermal Fluctuations of the DNA/PNA Geometry. The values of the squared electronic couplings computed using eq 1 along the MD trajectory are shown in Figure 1a for DNA and Figure 1b for PNA. The values of $\langle V_{DA}^2 \rangle$ were calculated to be 4.05×10^{-5} eV^2 for DNA and 4.45×10^{-5} eV^2 for PNA. However, these averages were significantly influenced by several MD snapshots

(59) Cheatham, T. E. *Curr. Opin. Struct. Biol.* **2004**, *14*, 360–367.
(60) Hagerman, P. J. *Annu. Rev. Biophys. Chem.* **1988**, *17*, 265–286.
(61) Olson, W. K.; Zhurkin, V. B. *Curr. Opin. Struct. Biol.* **2000**, *10*, 286–297.
(62) Dickerson, R. E.; Bansal, M.; Calladine, C. R.; Diekmann, S.; Hunter, W. N.; Kitzing, E. V.; Lavery, R.; Nelson, H. C. M.; Olson, W. K.; Saenger, W.; Shakked, Z.; Sklenar, H.; Soumpasis, D. M. *EMBO J.* **1989**, *8*, 1–4.
(63) Petersson, B.; Nielsen, B. B.; Rasmussen, H.; Larsen, I. K.; Gajhede, M.; Nielsen, P. E.; Kastrup, J. S. *J. Am. Chem. Soc.* **2005**, *127*, 1424–1430.
(64) Sen, S.; Nilsson, L. *J. Am. Chem. Soc.* **1998**, *120*, 619–631.

with V_{DA}^2 values several orders of magnitude larger than the average, up to 1.19×10^{-2} eV^2 for DNA and 1.52×10^{-2} eV^2 for PNA. In Figure 1, those few peaks dominate the plots, making the small-scale fluctuations of V_{DA}^2 all but invisible. Excluding just the single largest peak from our series decreased $\langle V_{DA}^2 \rangle$ by 20% (to 3.26×10^{-5} eV^2) for DNA and 23% (to 3.44×10^{-5} eV^2) for PNA.

A similar picture was observed earlier by Voityuk[29] for a GTG sequence, for which $\langle V_{DA}^2 \rangle$ over a 10 ps-long MD trajectory was calculated to be 3.9×10^{-4} eV^2 while the maximum V_{DA}^2 value reached $\sim 1.3 \times 10^{-2}$ eV^2. The $\langle V_{DA}^2 \rangle$ value for the shorter GTG sequence should indeed be an order of magnitude larger than that for our longer CATG sequence, consistent with the experimental CT rate decay constant[18,23] of 0.6 Å^{-1} (although the comparison is somewhat indirect because of the different geometries of intrastrand CT in ref 29 and the interstrand CT here). However, to find the maximum V_{DA}^2 values for the two sequences to be comparable is quite surprising. The structural origins of the large coupling peaks are explored further in the next section, as are the consequences for the hole-transport mechanism.

To place the above values into perspective, we computed $\langle V_{DA}^2 \rangle$ for the canonical B-DNA structure of our CATG sequence. The six-state GMH computations yielded a value of 7.1×10^{-7} eV^2 (compared to 3.6×10^{-6} eV^2 for the GTG sequence[29]). Such a significant difference from the $\langle V_{DA}^2 \rangle$ value computed over the MD trajectory proves that the thermal fluctuations of the DNA structure play a crucial role in the CT.

C. Evidence for Hopping CT at Short (2 BP) Donor−Acceptor Separations. In order to probe the structural origins of the large coupling values, we used the INDO/s data to compute the energies of the top occupied molecular orbitals of the core segment (HOMO through HOMO-2) and to visualize the localizations of those orbitals. Figure 2 shows the spatial distribution of those orbitals for two DNA and two PNA snapshots, first for structures with typically small V_{DA} values and then for structures with the largest V_{DA} values observed. The small-V_{DA} structures shown in Figure 2A,C correspond to DNA snapshot 101 ($V_{DA}^2 = 1.13 \times 10^{-9}$ eV^2) and PNA snapshot 1406 ($V_{DA}^2 = 3.06 \times 10^{-10}$ eV^2). Those structures have the HOMO density localized predominantly on one G, the HOMO-1 density on the other G, and the HOMO-2 density on one of the bridging As, as expected for the classical donor−bridge−acceptor picture. The highest-V_{DA} structures, corresponding to DNA snapshot 726 ($V_{DA}^2 = 1.19 \times 10^{-2}$ eV^2) and PNA snapshot 1350 ($V_{DA}^2 = 1.52 \times 10^{-2}$ eV^2) are shown in Figure 2B,D. In contrast to the small-V_{DA} case, the large-V_{DA} structures reveal a significant amount of HOMO and HOMO-1 density on the bridging bases. In DNA snapshot 726, both the HOMO and HOMO-1 are delocalized between a G and its neighboring A, whereas the HOMO-2 is localized on the G at the opposite end of the DNA segment. In PNA snapshot 1350, the HOMO is localized on one G, the HOMO-1 on the adjoining A, and the HOMO-2 on the other G.

The significant delocalization of the electron density onto the bridge in these structures indicates that the bridging states come into resonance with the donor or acceptor, thereby violating the basic GMH assumption that the bridge is energetically well-separated from the donor and acceptor.[54] *The CT in these special structures will not occur via a pure G-to-G superexchange route; instead, the hole will transfer from a G to the bridge, initiating CT via a hopping mechanism. In such cases, the application of eq 1* yields the coupling V_{12} between the HOMO and HOMO-1 rather than the coupling V_{DA} between the donor and acceptor states localized to the two Gs, and $V_{DA} \neq V_{12}$.

The electron-density distributions in all of the 1500 DNA and PNA snapshots were also analyzed. In all of the largest-V_{12} snapshots, more than 10% of the total charge density of either HOMO or HOMO-1 is delocalized onto the bridge. Conversely, every occurrence of a HOMO/HOMO-1 delocalization onto the bridge resulted in a large V_{12} value. Figure 3 lists all of the observed HOMO and HOMO-1 localization patterns for PNA and DNA. Overall, 17 different patterns were found, and the number of occurrences of each kind is different for DNA versus PNA. This likely reflects differences in the structural fluctuations of DNA and PNA. For example, case IX in Figure 3, where the donor is delocalized between the two A's and the acceptor is on a G, was seen in 5 snapshots for DNA but not observed in any of the 1500 PNA snapshots analyzed here. In contrast, case VI, where the donor is mixed between a G and the adjoining A and the acceptor is located on the other G, is seen in 168 PNA snapshots but only 61 DNA snapshots. In a few snapshots, the donor and acceptor were observed to be delocalized over three bases, spanning the entire length of the DNA/PNA sequence (e.g., cases XIV and XV in Figure 3). One can assume that a longer MD run with increased sampling might capture even rarer structures with more extensive delocalization.

D. Donor−Acceptor Coupling in the Superexchange Snapshots. Figure 4 plots V_{DA}^2 values for the subset of snapshots that conform to the direct G-to-G superexchange CT mechanism, i.e., those where the HOMO and HOMO-1 are localized on the Gs (case I in Figure 3). There are 1358 such snapshots for DNA and 1230 for PNA. The average coupling $\langle V_{DA}^2 \rangle = \langle V_{12}^2 \rangle$ computed for these snapshots was 1.02×10^{-6} eV^2 for DNA and 3.52×10^{-6} eV^2 for PNA, both of which are much lower than the values resulting from the full-trajectory average. The largest V_{DA}^2 values of the superexchange snapshots (1.99×10^{-4} eV^2 for DNA and 5.19×10^{-4} eV^2 for PNA) were also very much less than those of the excluded highest-V_{12}^2 peaks. The drastic influence of the $V_{12} \neq V_{DA}$ snapshots on $\langle V_{DA}^2 \rangle$ shows that it is essential to conduct an orbital delocalization analysis prior to computing the superexchange coupling interactions using the GMH approach. This conclusion is quite general and applies to any calculation using the GMH method or other formalisms to calculate electronic couplings.

Even for these "pure superexchange" snapshots, the V_{DA}^2 landscape is again dominated by the high peaks corresponding to values that are 2 orders of magnitude greater than the adjusted average (see Figure 4). It should be noted that the choice of a 10% delocalization threshold to separate the snapshots into superexchange and hopping groups is somewhat arbitrary. Delocalization of the HOMO and/or HOMO-1 onto the bridge by less than 10% can still increase the coupling dramatically, giving rise to the observed peaks. A more detailed analysis of the effect of orbital delocalization on the CT rate and mechanism is beyond the scope of this paper and will be addressed in the future.

As a final point of reference for these findings, we computed V_{DA}^2 values for the "ideal" structures of CATG DNA built using *model.it*,[47] which takes into account known sequence-specific structural variations of DNA derived from various experiments (Table 2). The ideal B-DNA structure, as well as the structure built on the basis of DNA gel-mobility data, conformed to the superexchange type discussed in this section and yielded V_{DA}^2 values of 7.1×10^{-7} and 5.9×10^{-8} eV^2, respectively. In

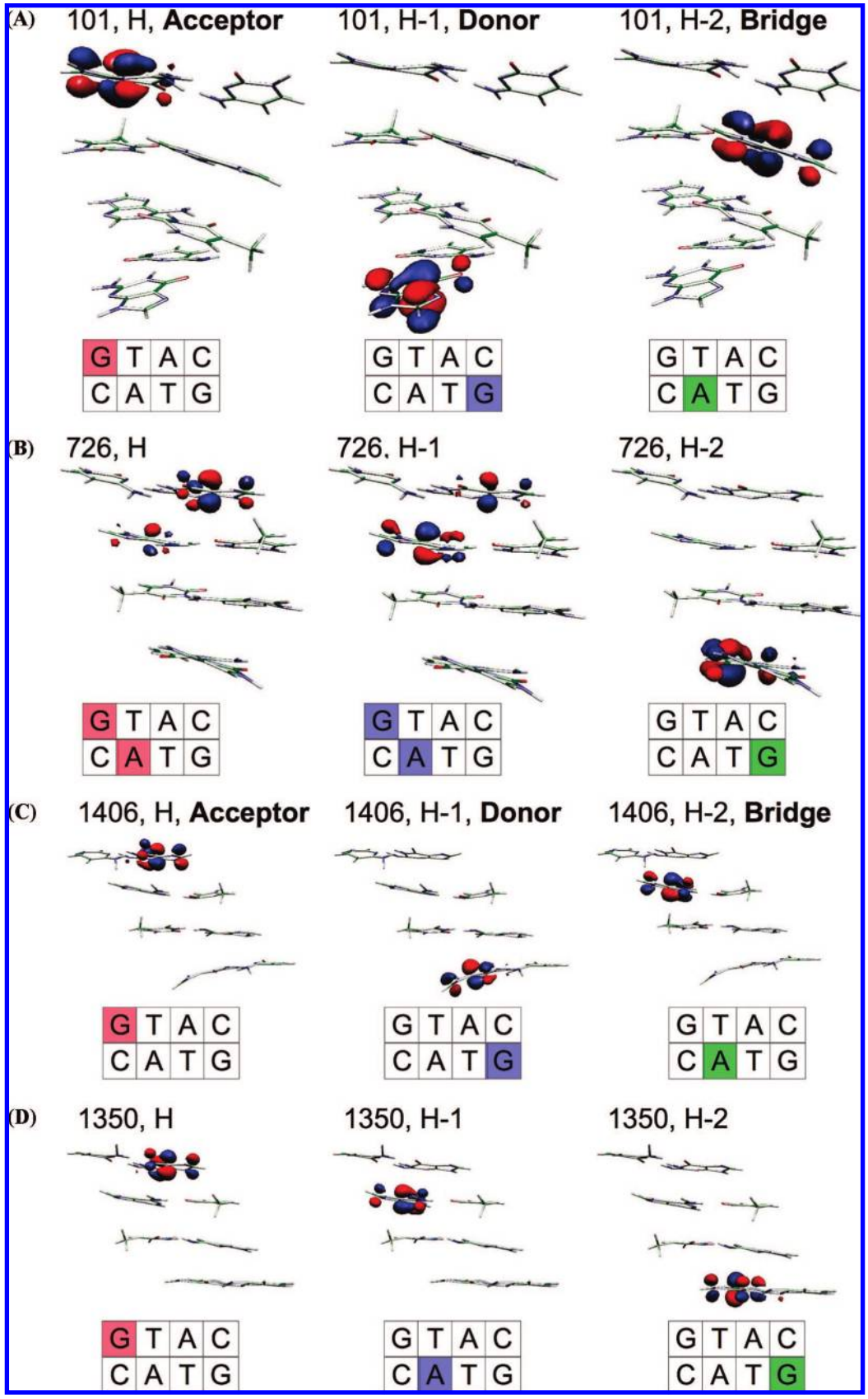

Figure 2. HOMO, HOMO-1, and HOMO-2 calculated with INDO/s for selected DNA and PNA snapshots: (A) DNA snapshot 101, (B) DNA snapshot 726, (C) PNA snapshot 1406, and (D) PNA snapshot 1350. The snapshots in (A) and (C) are typical representatives of small-V_{DA} structures, where the HOMO and HOMO-1 are localized to the two Gs. The snapshots in (B) and (D) correspond to the highest values of V_{12} calculated along the DNA and PNA MD trajectories and accordingly reveal a high degree of orbital delocalization to the bridge. The color of each orbital lobe corresponds to the phase of the wave function. The plots were prepared with MOLEKEL 4.3.[75,76]

Case number	Number of DNA snapshots	Number of PNA snapshots	
I	1358	1230	
II	27	12	
III	4	0	
IV	2	1	
V	22	6	
VI	61	168	
VII	9	2	
VIII	6	55	
IX	5	0	
X	6	12	
XI	5	2	
XII	2	9	
XIII	3	0	
XIV	1	1	
XV	0	1	
XVI	0	1	
XVII	0	1	

Figure 3. Classification of the DNA and PNA snapshots based on the HOMO and HOMO-1 distributions among the nucleic bases of the CATG segment. Red indicates the bases on which the HOMO (acceptor) density is significant, blue the bases on which the HOMO-1 (donor) density is significant, and purple the bases with a significant density of both HOMO and HOMO-1. The presence of an orbital on a given base is considered to be significant if at least 10% of the charge density of that orbital is present on that base.

contrast, both the structure based on NMR data and the "consensus" structure based on DNase I digestion and nucleosome positioning data exhibited significant delocalization of HOMO-1 and/or HOMO onto the bridge. These results once again clearly demonstrate the complex influence of structural variations on the electronic properties of DNA, emphasizing the importance of delocalization analysis when computing the DNA/PNA CT properties.

E. Origin of Orbital Localization/Delocalization. In order to understand which structural fluctuations of PNA and DNA drive the HOMO/HOMO-1 delocalization, we analyzed the correlation between V_{12} (and/or the degree of delocalization of HOMO/HOMO-1) and various structural metrics. No correlation was found between the electronic properties and many of the probed structural metrics, including the RMSD from the average structure or the initial DNA structure, the arc length along the DNA helix, the overlap area between the neighboring BPs, the standard helicoidal parameters (roll, tilt, twist, shift, slide, rise), and the BP conformational parameters (buckle, propeller, opening, shear, stretch, stagger). Similarly, no simple correlations were observed in earlier studies.[30]

Next, we analyzed the energies of the orbitals computed for isolated A and G bases extracted from the MD snapshots.

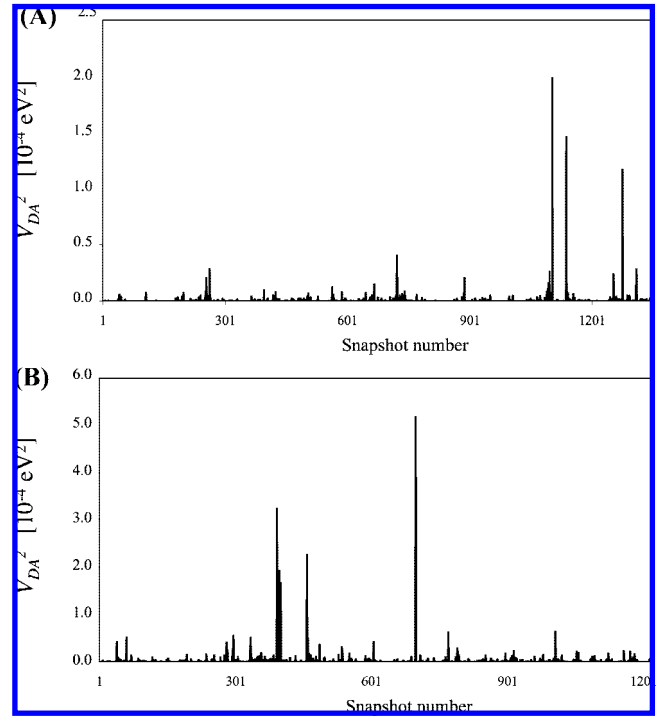

Figure 4. Squared electronic couplings V_{DA}^2 calculated using eq 1 for the subset of "superexchange" snapshots, in which the HOMO and HOMO-1 are localized on the G bases, as defined in Figure 3: (A) 1358 DNA snapshots, (B) 1230 PNA snapshots.

Gaussian distributions with $\sigma \approx 0.1$ eV were observed for the HOMO and HOMO-1 energies of each base (Figure 5A). The orbital energy distributions for G_1 and G_2 and also those for A_1 and A_2 overlap very closely. The HOMO energies of the Gs were shifted upward from the HOMO energies of the As by $\sim$0.25 eV, and the HOMO-1 energies of the Gs were shifted downward from the HOMO-1 energies of the As, as expected. However, a significant overlap between the G and A HOMO energy distributions was seen, suggesting that thermal fluctuations may indeed bring the energies into resonance and result in the observed orbital delocalization. A direct look at the energy gap $\Delta E(\text{G-A}) = E_{\text{HOMO,G}} - E_{\text{HOMO,A}}$ between the HOMOs of the Gs and As shows over a hundred resonant structures with vanishing energy gaps (Figure 5B). We conclude that the local fluctuations shift the hole energy levels on the individual bases and may bring the donor/acceptor into degeneracy with the bridge.

The Marcus theory of ET describes the distribution of donor/acceptor energy fluctuations induced by the dielectric medium.[65] Hopfield[66] framed these energy fluctuations in terms of spectral functions with standard deviations $\sigma = (\lambda k_B T)^{1/2}$, where λ is the reorganization energy. For reorganization energies on the order of 1 eV, these energy fluctuations are expected to be on the order of 0.1−0.2 eV, exactly as observed in our simulations and comparable to the computed energy gap between the isolated bases. On the basis of these tenets of ET theory, fluctuations of the bridging states into degeneracy with donor and acceptor states are indeed expected to be frequent,[65,66] as we have found. These observations are also consistent with the results of other studies[67−69] that classified the bridge-mediated CT into coherent

(65) Marcus, R. A.; Sutin, N. *Biochim. Biophys. Acta* **1985**, *811*, 265–322.
(66) Hopfield, J. J. *Proc. Natl. Acad. Sci. U.S.A.* **1974**, *71*, 3640–3644.

Table 2. Molecular Orbital Properties of the "Ideal" Structures of CATG DNA Built with *model.it*[47] on the Basis of Data on Sequence-Specific Structural Variations in DNA Derived from Various Experiments

model type	E_{HOMO} (eV)	E_{HOMO-1} (eV)	HOMO localization [amount (%)]	HOMO-1 localization [amount (%)]	V_{12}^2 (two-state GMH) (eV^2)	V_{12}^2 (six-state GMH) (eV^2)
B-DNA	−6.999	−6.993	G_2 [97.9]	G_1 [97.9]	1.2×10^{-7}	7.1×10^{-7}
gel-mobility based	−7.021	−7.040	G_2 [99.8]	G_1 [99.7]	7.4×10^{-8}	5.2×10^{-8}
NMR-based	−6.947	−6.968	G_2 [97.8]	G_1/A_2 [66.3/32.4]	5.9×10^{-7}	1.0×10^{-7}
"consensus"	−6.782	−6.809	G_2/A_1 [81.0/10.6]	$A_2/G_1/G_2$ [53.8/27.1/15.4]	9.8×10^{-5}	1.2×10^{-4}

and incoherent channels by comparing the time scales of intermediate bridge-state population (proportional to the inverse of the donor−bridge energy separation) and the bath dephasing time (arising from coupling of electronic states to vibrational motion). It is critical to distinguish the mechanism at play in DNA and PNA (i.e., the fluctuation of state energies because of coupling to nuclear degrees of freedom) from effects that may arise from simple Boltzmann population statistics for a static manifold of states.

Which structural fluctuations have the largest influence on the electronic energies of the ET-active orbitals? The HOMO/HOMO-1 energies of the isolated bases showed no correlation with either the planarity of the bases or the RMSDs of the bases from their average structures. However, a substantial correlation was found between the HOMO energies and the individual bond lengths (see the Supporting Information). Both G and A showed a pattern of bond alternation (Figure 6) in which the bonds whose lengths are positively correlated with the HOMO energy (colored red in Figure 6) alternate with those whose lengths are negatively correlated with the HOMO energy (colored blue in Figure 6). Presumably, the changes in the HOMO energy result from the larger (smaller) orbital delocalization over the aromatic base that stabilizes (destabilizes) the HOMO. These fluctuations are purely local and uncorrelated between the bases. Conceivably, other fluctuations of the medium that affect the HOMO delocalization in individual bases might also correlate with the HOMO energy levels.

This view that CT in DNA/PNA is gated by local conformational fluctuations is complementary to other effects studied in this field. For example, Barnett et al.[5] demonstrated an ion-gating mechanism for hole transport in a "frozen" DNA structure, and Voityuk and co-workers[70] showed that motion of the hydrogen atoms involved in the Watson−Crick

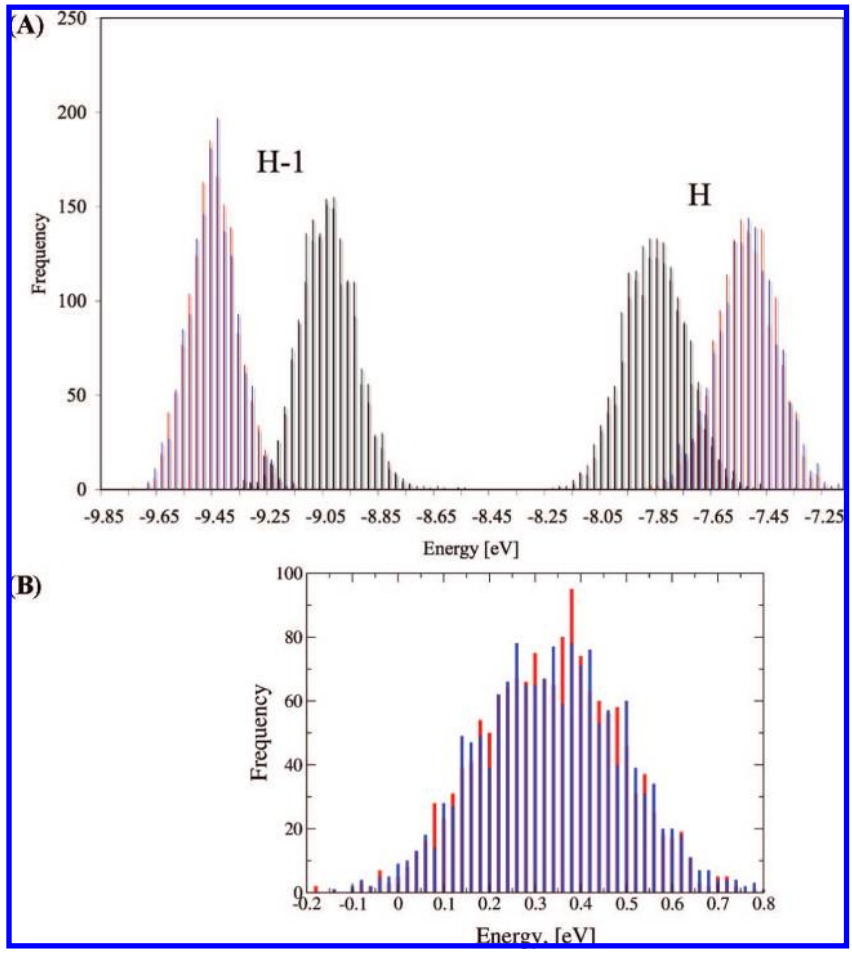

Figure 5. (A) The HOMO and HOMO-1 energies of the isolated DNA bases exhibit Gaussian distributions: A_1, black; A_2, gray; G_1, red; G_2, blue. The plots for the energies of A_1 and A_2 and those for G_1 and G_2 overlap almost completely, indicating adequate sampling of the energy values. The same picture is found for PNA (see the Supporting Information). (B) Distributions of the energy gaps ΔE(G-A) = $E_{HOMO,G} - E_{HOMO,A}$ between the HOMOs of the Gs and their neighboring As: blue, $\Delta E(G_2{:}A_1)$; red, $\Delta E(G_1{:}A_2)$.

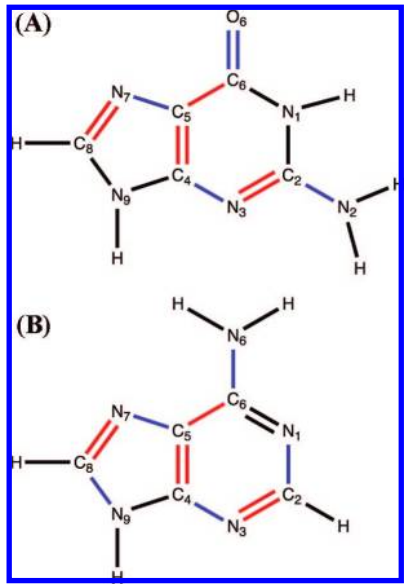

Figure 6. Correlation between individual bond lengths and the HOMO energies of the isolated bases in (A) guanine and (B) adenine. Bonds colored in red are positively correlated with E_{HOMO} (i.e., increasing the lengths of these bonds destabilizes the HOMO and increases E_{HOMO}). Bonds colored in blue are negatively correlated with E_{HOMO} (i.e., increasing their bond lengths stabilizes the HOMO and decreases E_{HOMO}).

hydrogen bonds may significantly affect the electronic structure of DNA base pairs. Both of these effects were excluded from the present study since (a) the explicit condensed-phase environment was not included in the INDO/s electronic structure analysis and (b) the lengths of the bonds between the hydrogens and the heavy atoms were frozen during the MD simulation. Nevertheless, we have found that fluctuations of the bond lengths between heavy atoms in the bases have as large an effect on the orbital distribution in DNA/PNA as the environmental fluctuations or the hydrogen motions. Thus, an accurate description of the electronic structures and CT properties of DNA and PNA should account for all of these effects. Notably, we observed conformational gating not only in DNA but also in PNA, where the effect of counterions should be negligible.

F. Comparison of Hole Transfer in PNA and DNA. Hopping and superexchange are the two limiting CT mechanisms. The results of the MD simulations presented here suggest that PNA possesses a higher CT rate than DNA in both regimes. For superexchange snapshots ($V_{DA} = V_{12}$), the calculated value of $\langle V_{DA}^2 \rangle$ for PNA (3.52×10^{-6} eV^2) was ~3.5 times larger than that for DNA (1.02×10^{-6} eV^2). This difference in V_{DA} values resulted mostly from the larger value of the adiabatic transition dipole moment μ_{12} (see eq 1) for PNA (0.23 D) than for DNA (0.09 D). This is consistent with the greater average geometric overlap between the neighboring Gs and As (8.59 Å^2 for PNA vs 0.65 Å^2 for DNA, as computed using X3DNA[71]), on which the value of μ_{12} directly depends. This difference in the overlap values is not unexpected for the studied sequence 5′-CATG-3′ and reflects the different relationship between base-pair shift and twist the in DNA and PNA geometries (see Scheme 1). On the basis of the difference in $\langle V_{DA}^2 \rangle$, we expect that the hole superexchange rates in PNA are likely to be several times larger than those in DNA, provided that other factors such as solvent reorganization energy are the same.

As far as the hopping mechanism is concerned, snapshots with significant charge density on the bridge ($V_{12} \neq V_{DA}$) occurred more frequently in PNA: 270 out of 1500 shapshots in PNA vs 142 out of 1500 snapshots for DNA (see Figure 3). We attribute this effect to the larger structural flexibility of PNA compared with DNA, which brings the bridge into resonance with the donor/acceptor states more frequently, even for the same degree of intra-base fluctuations. This view is strongly supported by experiments in DNA−ethidium systems,[72] where the CT rates for noncovalently attached (flexible) ethidium intercalator can be 4−5 orders of magnitude larger than those for covalently attached (more rigid) intercalators. We therefore expect CT rates in both the hopping and superexchange regimes to be larger in PNA than in DNA.

Conclusions

The electronic coupling for hole transfer in PNA and DNA was computed over a 1.5 ns MD trajectory. In agreement with earlier studies, we found that the thermal fluctuations of the helical structure significantly increase the nonadiabatic donor−acceptor coupling V_{DA} for hole-mediated superexchange. An analysis of the electronic structure of MD snapshots revealed a significant hole density on the bridge in ~10% of the snapshots. This finding indicates that the "superexchange only" view of CT for short DNA segments is incomplete and that CT by a hopping mechanism may contribute significantly to the overall kinetics, even for short (1−2 BP) bridges. Our results suggest that CT in DNA/PNA is gated by local conformational fluctuations: bond-length changes in the bases that change the localization/delocalization of the bases' frontier orbitals. This view is complementary to those of other studies in the field, which address the effect of proton transfer between base pairs,[70,73] ion gating,[5] and solvent gating[74] on DNA CT. The average squared coupling in PNA was found to be larger than in DNA, as was the frequency of hole delocalization to the bridge, suggesting a higher overall rate of CT in PNA than in DNA. Ongoing studies are likely to test these predictions in both single-molecule and ensemble experiments.[40,41]

Acknowledgment. This paper is dedicated to Tom Netzel. Financial support from the National Science Foundation (CRC Grant CHE-0628218) is gratefully acknowledged. We thank Prof. Jeffrey R. Reimers for the CNDO computer code. We also thank Profs. Gary Schuster, Alexander Voityuk, and Bob Cave for stimulating interactions.

Supporting Information Available: Atomic PNA charges used in the MD simulation; RMSD maps for PNA and DNA; plots

(67) Hu, Y. M.; Mukamel, S. *J. Chem. Phys.* **1989**, *91*, 6973–6988.
(68) Sumi, H.; Kakitani, T. *J. Phys. Chem. B* **2001**, *105*, 9603–9622.
(69) Sumi, H.; Kakitani, T. *Chem. Phys. Lett.* **1996**, *252*, 85–93.
(70) Rak, J.; Makowska, J.; Voityuk, A. A. *Chem. Phys.* **2006**, *325*, 567–574.
(71) Lu, X. J.; Olson, W. K. *Nucleic Acids Res.* **2003**, *31*, 5108–5121.
(72) Valis, L.; Wang, Q.; Raytchev, M.; Buchvarov, I.; Wagenknecht, H. A.; Fiebig, T. *Proc. Natl. Acad. Sci. U.S.A.* **2006**, *103*, 10192–10195.
(73) Boero, M.; Gervasio, F. L.; Parrinello, M. *Mol. Simul.* **2007**, *33*, 57–60.
(74) Mantz, Y. A.; Gervasio, F. L.; Laino, T.; Parrinello, M. *Phys. Rev. Lett.* **2007**, *99*, 058104.
(75) Flukiger, P.; Luthi, H. P.; Portmann, S.; Weber, J. MOLEKEL 4.3; Swiss National Supercomputing Center: Manno, Switzerland, 2002.
(76) Portmann, S.; Luthi, H. P. *Chimia* **2000**, *54*, 766–770.

showing correlations between HOMO energy/delocalization in the DNA/PNA segments and various structural metrics; histograms of E_{HOMO} and E_{HOMO-1} for the individual purine bases of PNA; plots showing no correlation between E_{HOMO} of individual DNA bases and selected chemical bond lengths; and a table of correlation coefficients of E_{HOMO} and the bond lengths for each DNA/PNA purine base. This material is available free of charge via the Internet at http://www.pubs.acs.org.

JA802541E